CHAPTER 16

Computational Restoration of Fluorescence Images: Noise Reduction, Deconvolution, and Pattern Recognition

Yu-li Wang

Department of Physiology
University of Massachusetts Medical School
Worcester, Massachusetts 01605

I. Introduction

Optical microscopy is now performed extensively in conjunction with digital imaging. A number of factors contribute to the limitations of the overall performance of the instrument, including the aperture of the objective lens, the inclusion of light originating from out-of-focus planes, and the limited signal-to-noise ratio of the detector. Both hardware and software approaches have been developed to overcome these problems. The former include improved objective lenses, confocal scanning optics, total internal reflection optics, and high-performance cameras. The latter, generally referred to as computational image restoration, include a variety of algorithms designed to reverse the defects of the optical-electronic system. The purpose of this chapter is to introduce in an intuitive way the basic concept of several computational image-restoration techniques that are particularly useful for processing fluorescence images.

METHODS IN CELL BIOLOGY, VOL. 72

0091-679X/03 $35.00

II. Adaptive Noise Filtration

Noise, defined as the uncertainty of intensity measurement, often represents the primary factor limiting the performance of both confocal microscopes and various computational approaches. Because of the statistical and accumulative nature of photon detection, noise may be reduced most effectively by increasing the time of image acquisition (Fig. 1A, B, G, H). However, this approach is often impractical for biological imaging because of the problems of sample movements, photobleaching, and radiation damage.

An optimal computational noise filter should aggressively remove random fluctuations in the image while preserving as much as possible the nonrandom features. Filters that apply a uniform algorithm across the image, such as low-pass convolution and median filters, usually lead to the degradation of image resolution or amplification of artifacts (Fig. 1). For example, low-pass filters cause both image features and noises to spread out over a defined area, whereas median filters replace every pixel with the median value of the neighborhood.

Better performance may be obtained using filters that adapt to the local characteristics of the image. In anisotropic diffusion filter (Black *et al.*, 1998; Tvarusko *et al.*, 1999), local intensity fluctuations are reduced through a simulated diffusion process by diffusing from pixels of high intensity toward neighboring pixels of low intensity. This process, when carried out in multiple iterations, effectively reduces intensity fluctuations by spreading the noise around a number of pixels. In one implementation (Black *et al.*, 1998), the change in intensity of a given pixel during a given iteration is calculated as

$$\lambda * \Sigma g(\Delta I)\Delta I, \tag{1}$$

where λ is a user-defined diffusion rate constant, ΔI is the difference in intensity from a neighboring pixel, and the sum Σ is taken over all eight neighbors. However, as diffusion without constraints would lead to homogenization of the entire image, it is critical to introduce the function $g(\Delta I)$ for the purpose of preserving structural features. In one of the algorithms, it is defined as $1/2[I - (\Delta I/\sigma)^2]^2$ when $|\Delta I|$ is $\leq\sigma$ and 0 otherwise (Black *et al.*, 1998). The constant σ thus defines a threshold of intensity transitions to be preserved as structures. If the difference in intensity is larger than σ, then diffusion is inhibited [$g(\Delta I) = 0$].

Although this diffusion mechanism works well in removing a large fraction of the noise, the recognition of features based on ΔI is not ideal, as it also preserves outlying noise pixels. The resulting "salt and pepper"-type noise (Fig. 2A, B) may have to be removed subsequently with a median filter. In an improved algorithm, the diffusion is controlled not by intensity differences between neighboring pixels but by edge structures detected in the images. If an edge is detected across a pixel (e.g., using correlation-based pattern recognition), then diffusion is allowed only along the edge; otherwise, diffusion is allowed in all directions. In essence, this

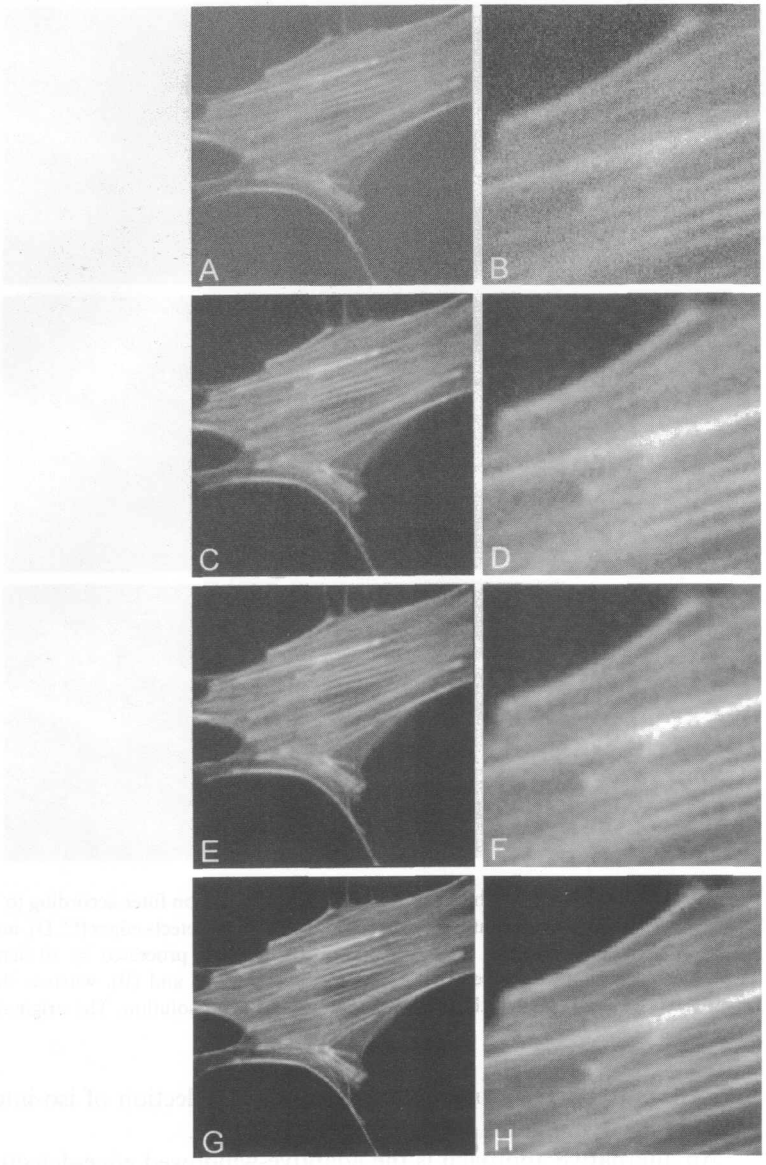

Fig. 1 Fluorescence images either unprocessed (A, B; G, H) or processed with a standard median filter (C, D) or low-pass convolution filter (E, F). Mouse fibroblasts were stained with rhodamine phalloidin, and images collected with a cooled CCD camera at a short (20 ms, A, B) or long (200 ms, G, H) exposure. A region of the cell is magnified to show details of noise and structures. Median filter creates a peculiar pattern of noise (C, D), whereas low-pass convolution filter creates fuzzy dots and a slight degradation in resolution (E, F).

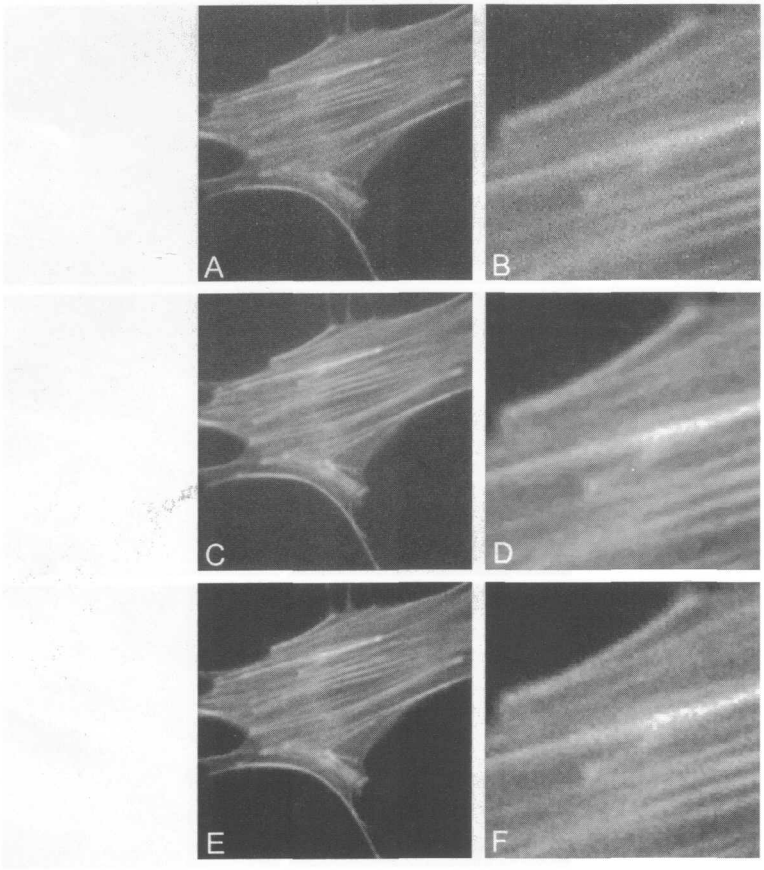

Fig. 2 Noise reduction with the original anisotropic diffusion filter according to Tukey (Black *et al.*, 1998; A, B), with a modified anisotropic diffusion filter that detects edges (C, D), and with an adaptive-window edge-detection filter (E, F). Images in (A–D) were processed by 10 iterations of diffusion. Residual noise outside the cell was easily noticeable in (A) and (B), whereas the noise was nearly completely removed in F without a noticeable penalty in resolution. The original image is shown in Fig. 1A and B.

algorithm treats structures in the image as a collection of iso-intensity lines that constrain the direction of diffusion (Fig. 2C, D).

An alternative approach is the adaptive-windowed edge-detection filter (Myler and Weeks, 1993). The basic concept is to remove the noise by averaging intensities within local regions, the size of which is adapted according to the local information content. In one implementation, the standard deviation of intensities is first calculated in a relatively large square region (e.g., 11×11) surrounding a pixel. If the standard deviation is lower than a defined threshold, indicating that no structure is present within the square, then the center intensity is replaced by the average value within the region and the calculation is moved to the next pixel.

Otherwise, the size of the square is reduced and the process is repeated. If the size of the square is eventually reduced to 3 × 3 and the standard deviation remains high, then the central pixel is likely located at a structural border. In this case an edge-detection operation is used to determine the orientation of the line, and the intensity of the central pixel is replaced by the average of the pixels that lie along the detected line. This procedure is repeated at each pixel of the image (Fig. 2E, F).

Both anisotropic diffusion and adaptive-window edge-detection methods can reduce the noise by up to an order of magnitude while preserving structural boundaries (Fig. 2). However, neither of them can restore lost resolution caused by high noise (cf Fig. 1G and H with Fig. 2). In addition, both of them preserve pseudofeatures formed by stochastic distribution of noise pixels. With anisotropic diffusion, areas of uniform signal may become populated with lumplike artifacts, whereas with adaptive-window edge-detection filters, straight bundle structures may show a jagged contour (Fig. 2). Despite these limitations, the reduction of noise alone can greatly improve the quality of noisy confocal images for three-dimensional reconstruction or for further processing (Tvarusko *et al.*, 1999).

III. Deconvolution

Mathematical reversal of systemic defects of the microscope is known as image "deconvolution." This is because the degradation effects of the microscope can be described mathematically as the "convolution" of input signals by the point-spread function of the optical system [Young, 1989; for a concise introduction of convolution, see the book by Russ (1994)]. The two-dimensional convolution operation is defined mathematically as

$$i(x,y) \otimes s(x,y) = \sum_{u,v} i(x-u, y-v)s(u,v). \tag{2}$$

This equation can be easily understood when one looks at the effects of convolving a matrix i with a 3 × 3 matrix:

$$\begin{array}{ll} \cdots\cdots\cdots\cdots & \\ \cdots\cdots i_1 i_2 i_3 \cdots\cdots & s_1 s_2 s_3 \\ \cdots\cdots i_4 i_5 i_6 \cdots\cdots & \otimes\ s_4 s_5 s_6 \\ \cdots\cdots i_7 i_8 i_9 \cdots\cdots & s_7 s_8 s_9. \\ \cdots\cdots\cdots\cdots & \end{array}$$

The calculation turns the element (pixel) i_5 into $(i_1 \times s_9) + (i_2 \times s_8) + (i_3 \times s_7) + (i_4 \times s_6) + (i_5 \times s_5) + (i_6 \times s_4) + (i_7 \times i_3) + (i_8 \times i_2) + (i_9 \times i_1)$. When calculated over the entire image, each pixel becomes "contaminated" by the surrounding pixels, to an extent specified by the values in the s matrix (the point-spread function). Thus, two-dimensional convolution operation mimics image degradation by the diffraction through a finite aperture. Three-dimensional convolution can be similarly expressed as

$$o(x,y,z) = i(x,y,z) \otimes s(x,y,z), \tag{3}$$

where $i(x,y,z)$ is three-dimensional matrix describing the signal originating from the sample, $s(x,y,z)$ is a matrix describing the three-dimensional point-spread function, which contains the information on image degradation caused by both diffraction and out-of-focus signals, and $o(x,y,z)$ is the stack of optical slices as detected with the microscope.

It should be noted that such precise mathematical description of signal degradation does not mean that original signal distribution can be restored unambiguously from the detected images and the point-spread function. Because of the loss of high-frequency information when light passes through the finite aperture of the objective lens, it is impossible to obtain predegraded images even under ideal conditions. The collected information instead allows a great number of potential "answers" to fit Eq. (3). This is because the calculation is plagued by a number of indeterminants as a result of "zero divided by zero." As a result, straightforward reversal of equation 3 (referred to as inverse filtering) typically leads to images that fit the mathematical criteria but contain unacceptable artifacts and amplified noise.

The challenge of computational deconvolution is to find strategies that identify the most likely answer. A number of deconvolution algorithms have been tested for restoring fluorescence images (for a detailed review, see Wallace *et al.*, 2001). The two main approaches in use are constrained iterative deconvolution (Agard, 1984; Agard *et al.*, 1989; Holmes and Liu, 1992) and nearest neighbor deconvolution (Castleman, 1979; Agard, 1984; Agard *et al.*, 1989). Constrained iterative deconvolution uses a trial-and-error process to look for signal distribution $i(x,y,z)$, that satisfies Eq. (3). It usually starts with the assumption that $i(x,y,z)$ equals the measured stack of optical sections, $o(x,y,z)$. As expected, when $o(x,y,z)$ is placed on the right-hand side of Eq. (3) in place of $i(x,y,z)$, it generates a matrix $o'(x,y,z)$ that deviates from $o(x,y,z)$ on the left-hand side. To decrease this deviation, adjustment is made to the initial guess, voxel by voxel, based on the deviation of $o'(x,y,z)$ from $o(x,y,z)$ and on constraints such as nonnegativity of voxel values. The modified $o(x,y,z)$ is then placed back into the right-hand side of Eq. (3) to generate a new matrix, $o''(x,y,z)$, which should resemble more closely $o(x,y,z)$ if the adjustment is made properly. This process is repeated until there is no further improvement or until the calculated image matches closely the actual image.

Various approaches have been developed to determine the adjustments in calculated images between iterations (Agard *et al.*, 1989; Holmes and Liu, 1992). Different algorithms differ with respect to the sensitivity to noise and artifact, speed to reach a stable answer, and resolution of the final image. Under ideal conditions, constrained iterative deconvolution can achieve a resolution that goes beyond what is predicted by the classical optical theory (Raleigh criterion) and provide three-dimensional intensity distribution of photometric accuracy (Carrington *et al.*, 1995). The main drawback of constrained iterative

deconvolution is its computational demand, which typically takes minutes to hours to complete a stack. This delay makes troubleshooting particularly tedious. A second disadvantage is its requirement for a complete stack of images for deconvolution, even if the experiment requires only one optical slice. Iterative constrained deconvolution is also very sensitive to the condition of the imaging, including optical defects and signal-to-noise ratio.

The nearest-neighbor algorithm is based on the decomposition of three-dimensional convolution [Equation (2)] into a series of two-dimensional convolutions (Agard *et al.*, 1989):

$$o(x,y) = i_0(x,y) \otimes s_0(x,y) + i_{-1}(x,y) \otimes s_{-1}(x,y) + i_{+1}(x,y) \otimes s_{+1}(x,y) + i_{-2}(x,y) \otimes s_{-2}(x,y) + i_{+2}(x,y) \otimes s_{+2}(x,y) + \cdots, \quad (4)$$

where $i(x,y)$'s are two-dimensional matrices describing the signal originating from the plane of focus (i_0), and from the planes above (i_{+1}, i_{+2}, ...) and below (i_{-1}, i_{-2}, ...), $s(x,y)$ are matrices of two-dimensional point-spread functions that describe how point sources on the plane of focus (s_0) or planes above (s_{+1}, s_{+2}, ...) and below (s_{-1}, s_{-2}. ...) spread out when they reach the plane of focus. This equation is further simplified by introducing three assumptions: first, that out-of-focus light from planes other than those adjacent to the plane of focus is negligible; that is, terms containing s_{-2}, s_{+2}, and beyond are insignificant. Second, that light originating from planes immediately above or below the plane of focus can be approximated by images taken while focusing on these planes; i.e., $i_{-1} \approx o_{-1}$ and $i_{+1} \approx o_{+1}$. Third, that point-spread functions for planes immediately above and below the focal plane, s_{-1} and s_{+1}, are equivalent (hereafter denoted as s_1).

These approximations simplify Eq. (4) into

$$o = i_0 \otimes s_0 + (o_{-1} + o_{+1}) \otimes s_1. \quad (5)$$

Rearranging the equation and applying Fourier transformation, the equation turns into

$$i_0 = [o - (o_{-1} + o_{+1}) \otimes s_1] \otimes F^{-1}[1/F(s_0)], \quad (6)$$

where F and F^{-1} represents forward and reverse Fourier transformation, respectively. This equation can be understood in an intuitive way: It states that the unknown signal distribution, i_o, can be obtained by taking the in-focus image, o, subtracting out estimated contributions from planes above and below the plane of focus, $(o_{-1} + o_{+1}) \otimes s_1$, followed by the convolution with the matrix $F^{-1}[1/F(s_0)]$ to reverse diffraction-introduced spreading of signals on the plane of focus.

To address artifacts introduced by the approximations, nearest-neighbor deconvolution is typically performed with a modified form of Eq. (6):

$$i_0 = [o - (o_{-1} + o_{+1}) \otimes (c_1 * s_1)] \otimes F^{-1}[F(s_0)/(F(s_0)^2 + c_2)], \quad (7)$$

where constants c_1 and c_2 are empirical factors. c_1 is used to offset errors caused by oversubtraction, as described below. c_2 is required to deal with problems associated with the calculation of reciprocals, $1/F(s_0)$, at the end of Eq. (6). The constant c_2 keeps the reciprocal value from getting too large when the matrix element is small compared to c_2. In general, c_1 falls in the range of 0.45 to 0.50, depending on the separation between adjacent optical slices, whereas the value of c_2 is in the range of 0.0001 to 0.001, depending on the level of noise in the images. The optimal values for c_1 and c_2 should be determined through systematic trials.

The main concern of nearest-neighbor deconvolution is its accuracy because of the three approximations discussed above. In particular, as the neighboring optical sections include significant contributions of signals from the plane of focus, the use of these images leads to oversubtraction and erosion of structures, particularly when the optical section is performed at too small a spacing. However, the approximations also greatly simplify and accelerate the calculations. It requires the collection of only three images (the in-focus image and images immediately above and below), which reduces photobleaching during image acquisition. Unlike constrained iterative deconvolution, the computation is finished within seconds. In addition, it is relatively insensitive to the quality of the lens or the point-spread function, yielding visually satisfactory results with either actual or computer-calculated point-spread functions. When the constant c_1 is set small enough, even the image itself may be used as an approximation of the neighbors. The resulting "no-neighbor" deconvolution is in essence identical to "unsharp-masking" found in many graphics programs such as Photoshop. Nearest-neighbor deconvolution can serve as a quick-and-dirty means for qualitative deblurring. It is ideal for preliminary evaluation of samples and optical sections, which may then be processed with constrained iterative deconvolution.

There are cases where confocal microscopy would be more suitable than either deconvolution techniques. Both contrained iterative and nearest-neighbor deconvolution require images of relatively low noise. Although noise may be reduced before and during the calculation with filters, as discussed earlier, in photon-limited cases, this may not give acceptable results. In addition, laser confocal microscopy is more suitable for thick samples, where the decreasing penetration and scattering of light limit the performance of deconvolution. For applications with moderate demand in resolution and light penetration, but high demand in speed and convenience, spinning disk confocal microscopy serves a unique purpose. Finally, under ideal situations, the combination of confocal imaging and deconvolution should yield the highest performance.

IV. Pattern Recognition–Based Image Restoration

Deconvolution as discussed above is based on few assumptions about the image. However, in many cases the fluorescence image contains specific characteristics, which may be used as powerful preconditions for image restoration. One such

example is the detection of microtubules in immunofluorescence or GFP images. The prior knowledge, that all the features in these images consist of line structures, allows one to take an alternative approach based on the detection of linear features.

Pattern recognition is performed most easily with a correlation-based algorithm. The correlation operation,

$$i(x,y) + (x,y) = \sum_{u,v} i(x+u, y+v)s(u,v), \tag{8}$$

is similar to that of convolution except that the corresponding (instead of transposed) elements from the two matrices are multiplied together; that is, when a matrix i is correlated with a 3×3 matrix, s,

$$\begin{array}{l} \cdots\cdots\cdots\cdots \\ \cdots\cdots i_1 i_2 i_3 \cdots\cdots \\ \cdots\cdots i_4 i_5 i_6 \cdots\cdots \\ \cdots\cdots i_7 i_8 i_9 \cdots\cdots \\ \cdots\cdots\cdots\cdots \end{array} \quad \begin{array}{l} \\ s_1 s_2 s_3 \\ + \; s_4 s_5 s_6 \; . \\ s_7 s_8 s_9 \\ \\ \end{array}$$

The element (pixel) i_5 turns into $(i_1 \times s_1) + (i_2 \times s_2) + (i_3 \times s_3) + (i_4 \times s_4) + (i_5 \times s_5) + (i_6 \times s_6) + (i_7 \times i_7) + (i_8 \times i_8) + (i_9 \times i_9)$.

It can be easily seen that this result is maximal when the two matrices contain an identical pattern of numbers, such that large numbers are multiplied by large numbers and small numbers multiplied by small numbers. The operation thus provides a quantitative map indicating the degree of match between the image (i) and the pattern (s) at each pixel. To make the calculation more useful, Eq. (8) is modified as

$$i(x,y) + (x,y) = \sum_{u,v} [i(x+u, y+v) - i_{\text{avg}}][s(u,v) - s_{\text{avg}}] \tag{9}$$

to generate both positive and negative results; negative values indicate that one matrix is the negative image of the other (i.e., bright regions correspond to dark regions, and vice versa).

Figure 3 shows the matrices $s(u,v)$ for detecting linear segments in eight different orientations. The operations generate eight correlation images, each one detecting segments of linear structures (microtubules) along a certain orientation. Negative correlation values are then clipped to zero, and the images are added together to generate the final image (Fig. 4). This is a much faster operation than iterative deconvolution, yet the results are substantially better than that provided by nearest neighbor deconvolution. However, despite the superb image quality, the method is not suitable for quantitative analysis of intensity distribution.

```
1.000 2.000 4.000 2.000 1.000
1.000 2.000 4.000 2.000 1.000
1.000 2.000 4.000 2.000 1.000
1.000 2.000 4.000 2.000 1.000
1.000 2.000 4.000 2.000 1.000


0.386 1.310 2.468 3.684 1.918
0.769 1.693 3.234 2.918 1.535
1.152 2.152 4.000 2.152 1.152
1.535 2.918 3.234 1.693 0.769
1.918 3.684 2.468 1.310 0.386


0.172 0.879 1.586 2.586 4.000
0.879 1.586 2.586 4.000 2.586
1.586 2.586 4.000 2.586 1.586
2.586 4.000 2.586 1.586 0.879
4.000 2.586 1.586 0.879 0.172


0.386 0.769 1.152 1.535 1.918
1.310 1.693 2.152 2.918 3.684
2.468 3.234 4.000 3.234 2.468
3.684 2.918 2.152 1.693 1.310
1.918 1.535 1.152 0.769 0.386


1.000 1.000 1.000 1.000 1.000
2.000 2.000 2.000 2.000 2.000
4.000 4.000 4.000 4.000 4.000
2.000 2.000 2.000 2.000 2.000
1.000 1.000 1.000 1.000 1.000


1.918 1.535 1.152 0.769 0.386
3.684 2.918 2.152 1.693 1.310
2.468 3.234 4.000 3.234 2.468
1.310 1.693 2.152 2.918 3.684
0.386 0.769 1.152 1.535 1.918


4.000 2.586 1.586 0.879 0.172
2.586 4.000 2.586 1.586 0.879
1.586 2.586 4.000 2.586 1.586
0.879 1.586 2.586 4.000 2.586
0.172 0.879 1.586 2.586 4.000


1.918 3.684 2.468 1.310 0.386
1.535 2.918 3.234 1.693 0.769
1.152 2.152 4.000 2.152 1.152
0.769 1.693 3.234 2.918 1.535
0.386 1.310 2.468 3.684 1.918
```

Fig. 3 Matrices for detecting linear structures lying along the directions of north–south, north–northeast, northeast, east–northeast, east–west, west–northwest, northwest, and north–northwest.

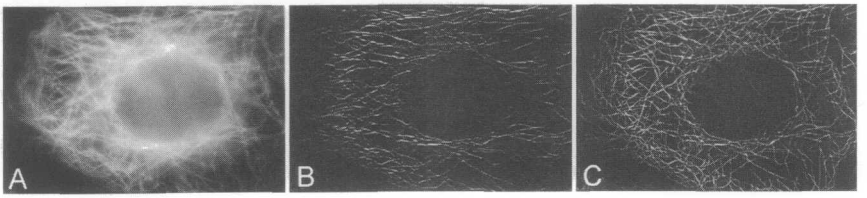

Fig. 4. Restoring of microtubules by feature recognition. An optical slice of a NRK cell stained for microtubules is shown in (A). The image is processed to detect linear segments lying along the east–west direction (B). A complete image, obtained by summing structures along all the eight directions, is shown in (C).

V. Prospectus

Image processing and restoration represent a rapidly advancing field of information science. However, not all the algorithms are equally suitable for fluorescence microscopic images, because of their special characteristics. As optical microscopy continues to push for maximal speed and minimal irradiation, overcoming the limitation in signal-to-noise ratio will likely remain a major challenge for both the retrieval of information from unprocessed images and the application of various restoration algorithms. Development of optimal noise-reduction algorithms represents one of the most urgent tasks for the years to come. Although this chapter explores several simple methods for noise reduction, new methods based on probability theories may be combined with deconvolution to overcome the resolution limit imposed by noise. In addition, as many biological structures contain characteristic features, the application of feature recognition and extraction will play an increasingly important role in both light and electron microscopy. The ultimate performance in microscopy will likely come from combined hardware and software approaches, for example, by spatial/ temporal modulation of light signals coupled with software decoding and processing (Gustafsson *et al.*, 1999; Lanni and Wilson, 2000).

References

Agard, D. A. (1984). *Ann. Rev. Biophys. Bioeng.* **13,** 191–219.

Agard, D. A., Hiraoka, Y., Shaw, P., and Sedat, J. W. (1989). *Methods Cell Biol.* **30,** 353–377.

Black, M. J., Sapiro, G., Marimont, D. H., and Heeger, D. (1998). *IEEE Trans. Image Process.* **7,** 421–432.

Carrington, W. A., Lynch, R. M., Moore, E. D., Isenberg, G., Fogarty, K. E., and Fay, F. S. (1995). *Science* **268,** 1483–1487.

Castleman, K. R. (1979). "Digital Image Processing" Prentice-Hall, Englewood Cliffs, NJ.

Gustafsson, M. G., Agard, D. A., and Sedat, J. W. (1999). *J. Microsc.* **195,** 10–16.

Holmes, T. J., and Liu, Y.-H. (1992). *In* "Visualization in Biomedical Microscopies" (A. Kriete ed.), pp. 283–327. VCH Press, New York.

Lanni, F., and Wilson, T. (2000). *In* "Neuron Imaging" (R. Yuster, A. Lanni, and A. Konnerth eds.), pp. 8.1–8.9. Cold Spring Harbor Laboratory Press, Cold Spring Harbor, NY.

Myler, H. R., and Weeks, A. R. (1993). "Computer Imaging Recipes in C." Prentice-Hall, Englewood Cliffs, NJ.

Russ, J. C. (1994). "The Image Processing Handbook." CRC Press, Boca Raton, FL.

Tvarusko, W., Bentele, M., Misteli, T., Rudolf, R., Kaether, C., Spector, D. L., Gerdes, H. H., and Eils, R. (1999). *Proc. Natl. Acad. Sci. USA* **96,** 7950–7955.

Wallace, W., Shaefer, L. H., and Swedlow, J. R. (2001). *BioTechniques* **31,** 1076–1097.

Young, I. T. (1989). *Methods Cell Biol.* **30,** 1–45.